Extensional flow of nematic liquid crystal with an applied electric field

L. J. CUMMINGS[1], J. LOW[2] and T. G. MYERS[1]

[1]*Department of Mathematical Sciences, New Jersey Institute of Technology, Newark, NJ 07102-1982, USA*
emails: `linda.j.cummings@njit.edu, tmyers@crm.cat`
[2]*Centre de Recerca Matemàtica, Campus de Bellaterra, Edifici C, 08193 Bellaterra, Barcelona, Spain*
email: `jlow@crm.cat`

Systematic asymptotic methods are used to formulate a model for the extensional flow of a thin sheet of nematic liquid crystal. With no external body forces applied, the model is found to be equivalent to the so-called Trouton model for Newtonian sheets (and fibres), albeit with a modified 'Trouton ratio'. However, with a symmetry-breaking electric field gradient applied, behaviour deviates from the Newtonian case, and the sheet can undergo finite-time breakup if a suitable destabilizing field is applied. Some simple exact solutions are presented to illustrate the results in certain idealized limits, as well as sample numerical results to the full model equations.

Key words: Nematic liquid crystal; Thin film; Viscous sheet; Electric field

1 Introduction

Nematic liquid crystals (NLCs) are ubiquitous in nature, and find wide applications in many industrial processes. For example, many modern display devices, certain thermometers and some biopathogen detection methods exploit the liquid crystalline nature of chemicals. Contemporary makeup products also often rely on various liquid crystal compounds for their iridescent optical qualities [12]. An understanding of how liquid crystals behave under a wide variety of conditions is thus commercially important, but due to the highly complex nature of the governing dynamic equations it can be challenging to investigate the behaviour theoretically from a mechanistic viewpoint. Simple experimental setups can be very valuable as an investigative tool to reveal novel behaviour and new regimes not exhibited by Newtonian fluids. For example, a system as simple as a spreading nematic droplet can exhibit highly complex fingering instabilities [13]. The mathematical models described recently in [9,10] reveal that these arise due to a complex interplay between fluid flow, internal elasticity and surface (anchoring) energy: strong anchoring will stabilize a film, but with weak anchoring the free surface can destabilize.

In this paper we investigate another simple experimental configuration: a thin nematic sheet with one end clamped and the other pulled, subject to a constant force or prescribed speed. This simple setup allows us to make analytical progress, which can aid our overall understanding of free-surface liquid crystal dynamics. We note that the analysis represents

a rare example of a tractable non-Newtonian extensional flow; other notable examples include King & Oliver's [8] analysis of an extensional poroviscous flow (with a novel application to the leading-edge protrusion of a cell crawling on a substrate), and the exact solution presented by Smolka *et al.* [16] for the extension of a viscoelastic filament.

Since liquid crystals are strongly affected by electric fields (a fact important for many of their applications), we also include an applied field in the formulation. With no applied field, we find that the nematic model reduces to the equivalent Newtonian problem, with just a change in the timescale. This Newtonian problem has been studied in detail, in particular in the context of glass manufacture, see Howell [5, 6] and many references therein. Axisymmetric instabilities of nematic fibres have been studied both experimentally and analytically by Savage *et al.* [15] and Cheong & Rey [14] but to date this work has not been extended to sheet flow. In fact, due to the simpler geometry of the sheet (which makes dealing with the free surface anchoring conditions on the nematic molecules easier), the model we obtain is more analytically tractable than that of Rey & Cheon [14].

The paper is set out as follows. In Section 2 we describe the mathematical model. The full description for the extensional flow of a nematic sheet is complex. Consequently we reduce the model systematically, in the spirit of Howell [5, 6], to obtain a closed system of governing equations describing the flow velocity u along the sheet's centreline, the sheet thickness h and the director angle θ. To simplify the problem further we make various standard assumptions concerning the elastic and 'viscous' constants and apply an electric field that to leading order has a component only in the cross-sheet direction (the asymptotic reduction of the electric field is discussed in Appendix A). We also give a brief discussion of suitable boundary conditions. Section 3 deals with simple explicit solutions of the reduced asymptotic model. Possible steady states in the presence of an electric field and their stability characteristics are considered. It is also shown that when surface tension effects are neglected, the model may be solved exactly in a certain limit, and specific cases of such solutions are presented. In Section 4 we carry out numerical simulations of the full unsteady model and explore the dependence on initial and boundary conditions and on electric field gradients. Finally, in Section 5 we present our conclusions.

2 The model

The details of the theory governing the flow of NLCs are well documented and provided in texts such as [2, 4, 8]. The notation we employ is mostly the same as that used by Leslie [8], the two main functions being the velocity field of the flow, $\boldsymbol{v} = (v_1, v_2, v_3) = (u, v, w)$, and the director field $\boldsymbol{n}$, the unit vector describing the orientation of the anisotropic axis in the liquid crystal (an idealized representation of the local preferred average direction of the rod-like liquid crystal molecules). The evolution of $\boldsymbol{n}$ is determined by elastic stresses within the NLC, by the local flow-field, and by any externally acting fields. In this paper we shall restrict attention to the 2D case in which flow and the director field are confined to the (x, z)-plane so that $\boldsymbol{v} = (v_1, 0, v_3) = (u, 0, w)$, and $\boldsymbol{n} = (\sin\theta, 0, \cos\theta)$, $\theta(x, z, t)$ being the angle the director makes with the z-axis. We also neglect inertia from the outset, since only slowly deforming sheets will be considered.

The governing equations in the bulk are:

$$\frac{\partial}{\partial x_i}\left(\frac{\partial W}{\partial \theta_{x_i}}\right) - \frac{\partial W}{\partial \theta} + \tilde{g}_i \frac{\partial n_i}{\partial \theta} = 0, \tag{1}$$

$$-\frac{\partial \pi}{\partial x_i} + \tilde{g}_k \frac{\partial n_k}{\partial \theta} + \frac{\partial \tilde{t}_{ik}}{\partial x_k} = 0, \tag{2}$$

$$\frac{\partial v_i}{\partial x_i} = 0, \tag{3}$$

representing energy, momentum and mass conservation respectively. The quantities $\tilde{g}$ and π are defined by

$$\tilde{g}_i = -\gamma_1 N_i - \gamma_2 e_{ik} n_k, \qquad e_{ij} = \frac{1}{2}\left(\frac{\partial v_i}{\partial x_j} + \frac{\partial v_j}{\partial x_i}\right), \tag{4}$$

$$N_i = \dot{n}_i - \omega_{ik} n_k, \qquad \omega_{ij} = \frac{1}{2}\left(\frac{\partial v_i}{\partial x_j} - \frac{\partial v_j}{\partial x_i}\right), \tag{5}$$

$$\pi = p + W, \tag{6}$$

where γ_1 and γ_2 are constants (viscosities), p is the pressure and W is the bulk energy, containing elastic and possible dielectric contributions. It is defined in terms of the director and the applied field by

$$2W = K_1(\nabla \cdot \boldsymbol{n})^2 + K_2(\boldsymbol{n} \cdot \nabla \wedge \boldsymbol{n})^2 + K_3((\boldsymbol{n} \cdot \nabla)\boldsymbol{n}) \cdot ((\boldsymbol{n} \cdot \nabla)\boldsymbol{n})$$
$$- \varepsilon\varepsilon_\perp \boldsymbol{E} \cdot \boldsymbol{E} - \varepsilon(\varepsilon_\| - \varepsilon_\perp)(\boldsymbol{n} \cdot \boldsymbol{E})^2, \tag{7}$$

where K_1, K_2 and K_3 are elastic constants, ε is the permittivity of free space and $\varepsilon_\|$ and $\varepsilon_\perp$ are the relative dielectric permittivities parallel and perpendicular to the long axis of the molecules. Finally, $\tilde{t}_{ij}$ is the extra-stress tensor (related to the stress σ_{ij} by $\sigma_{ij} = -\pi\delta_{ij} + \tilde{t}_{ij}$)

$$\tilde{t}_{ij} = \alpha_1 n_k n_p e_{kp} n_i n_j + \alpha_2 N_i n_j + \alpha_3 N_j n_i + \alpha_4 e_{ij} + \alpha_5 e_{ik} n_k n_j + \alpha_6 e_{jk} n_k n_i, \tag{8}$$

where α_i are constant, although not necessarily positive, viscosities (they are related to γ_i in (4) by $\gamma_1 = \alpha_3 - \alpha_2$ and $\gamma_2 = \alpha_6 - \alpha_5$) and $\mu = \alpha_4/2$ corresponds to the dynamic viscosity in the standard Newtonian (isotropic) case when all other α_i are zero.

Equation (1) is the energy equation. The first three terms in the bulk energy W (defined in (7)) represent the elastic energy associated with the director field; and the last two represent the tendency of the director to align parallel to an applied electric field $\boldsymbol{E}$ (when $\varepsilon_\| > \varepsilon_\perp$). The three elastic contributions to W are known as splay, twist and bend respectively, and represent energy penalties incurred when the director field has local behaviour of these types [4]. Note that the so-called saddle-splay term (see e.g. [2, 4, 17]) that often appears in the elastic energy, with associated elastic constant K_{24}, is identically zero for a two-dimensional (2D) director field of the kind we consider.

The model must be solved subject to appropriate boundary conditions. For a stretched sheet with free surfaces, these are: a stress balance condition that equates the stress vector at each sheet surface to any external forces acting; a kinematic condition at each sheet surface; and an anchoring condition on the director field at each of the free surfaces. We
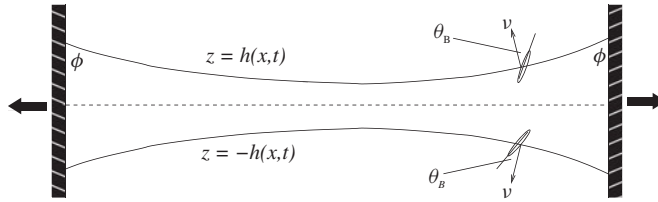
FIGURE 1. Schematic of a nematic sheet under stretching from its ends. The preferred anchoring angles at the two surfaces are also indicated. Further details may be found in the text.

will consider a situation where the sheet is stretched between two plates, one of which is fixed. The other is pulled either with a prescribed velocity or a prescribed force. With non-zero surface tension we also impose a contact angle ϕ between the fluid and plate (see Appendix B for further discussion of this condition). In general, the upper and lower surfaces of a 2D fluid sheet may be described by equations $z = H(x,t) \pm h(x,t)/2$, where $z = H(x,t)$ represents the sheet centreline, and $h(x,t)$ represents the sheet thickness. A definition sketch for the pulled sheet is shown in Figure 1 for the case in which the sheet centreline is flat (this turns out to be generic).

The stress balance then takes the form

$$\boldsymbol{\sigma} \boldsymbol{v}^{\pm} = -\hat{\gamma} \kappa^{\pm} \boldsymbol{v}^{\pm} \quad \text{on } z = H \pm h/2, \tag{9}$$

where $\sigma_{ij} = -\pi \delta_{ij} + \tilde{t}_{ij}$ is the stress tensor, $\boldsymbol{v}^{\pm}$ is the outward normal vector to the free surface $z = H \pm h/2$, $\kappa^{\pm}$ is its curvature and $\hat{\gamma}$ is a coefficient of surface tension. The kinematic condition states

$$\boldsymbol{v} \cdot \boldsymbol{v}^{\pm} = V_{v}^{\pm} \quad \text{on } z = H \pm h/2, \tag{10}$$

where $V_{v}^{\pm}$ is the outward normal velocity of the interface $z = H \pm h/2$.

The director field satisfies 'anchoring' boundary conditions at a free surface, which model its tendency to align at a certain angle, θ_B, to the normal $\boldsymbol{v}$ (θ_B is the angle that minimizes surface energy for the system in the absence of applied fields). In a 3D context this represents conical anchoring: the director lies on a cone of angle θ_B. Within our 2D model this means that the director can take values $\pm \theta_B$ at either interface. For a sheet, the normals at the two surfaces point in different directions, and the anchoring angles will be selected so as to give the overall lowest energy – thus, if θ_B is selected at the upper interface, it will also be selected at the lower interface (bearing in mind the different orientations of the normals at two surfaces); see Figure 1. Assuming this situation, we model it by an *ad hoc* anchoring condition which says that in the absence of an applied field the director will take the preferred direction, but that an applied field will act to pull the director angle towards the field direction. If the applied electric field has the form

$$\boldsymbol{E} \approx a(x) \boldsymbol{e}_z \tag{11}$$

(this is justified in detail in Appendix A), then we take

$$\theta = \theta_B g(a(x)) \quad \text{on } z = H \pm h/2. \tag{12}$$

The choice of function g is somewhat arbitrary. It must be monotonically decreasing in a and tend to zero for large a in order to align the director fully with the field. The form that we assume for all of our example calculations in this paper is

$$g(a) = \frac{E_a^2}{a^2 + E_a^2} \tag{13}$$

for some $E_a > 0$ (an alignment field strength sufficient to overcome the surface anchoring). This anchoring condition is only approximate, since in the absence of a field it gives $\theta = \theta_B$ (that is, the angle between the director and the vertical takes the value θ_B). In reality it should be the angle between $\boldsymbol{n}$ and the normal to the surface $\boldsymbol{v}$ that takes the value θ_B. However, in our subsequent asymptotic approximation $\boldsymbol{v} \approx \pm(0, 1)$, so that condition (12) is correct to the required order.

2.1 Scaling and non-dimensionalisation

The experimental setup modelled is a thin 2D sheet of NLC extended from its ends. The Newtonian analogue has been considered by several authors. We follow the approach of Howell [5,6], but see also van de Fliert *et al.* [18] and the many references within these papers for other asymptotic work on the Newtonian problem. In the previous section we set out the problem for the general case where the NLC film occupies the region between the two free surfaces $z = H \pm h/2$. However, as in the Newtonian case [5,6], our analysis reveals that the centreline is straight to leading-order for any sheet with positive tension.[1] We shall therefore simplify the presentation by making this assumption from the outset (the details of how this result is derived are similar to the Newtonian case, but complicated by the presence of the director angle in the model).

To derive systematic asymptotic approximations to the governing equations, we introduce appropriate scalings for the flow variables as follows [11]:

$$(x, z) = L(\tilde{x}, \delta\tilde{z}), \ (u, w) = U(\tilde{u}, \delta\tilde{w}), \ t = \frac{L}{U}\tilde{t}, \ \pi = \frac{\mu U}{L}\tilde{p}, \tag{14}$$

where L is the length scale of typical variations in the x-direction (for example, it could be the initial length of the sheet); U is a typical flow velocity along the sheet axis (fixed, e.g. by pulling on the sheet's ends); $\delta = \hat{h}/L \ll 1$ is a typical aspect ratio of the sheet ($\hat{h}$ being a typical sheet thickness) and $\mu \equiv \alpha_4/2 > 0$ is the representative viscosity scaling in the pressure (since this corresponds to the usual viscosity in the isotropic case in (8)).[2] We also write $h = \hat{h}\tilde{h}$ to define the dimensionless sheet width.

If $K = K_1$ is a representative value of the elastic constants K_1, K_2, K_3, then (7) gives the appropriate scaling for W as

$$W = \frac{K}{\delta^2 L^2}\tilde{W},$$

[1] This is true at least on any timescale relevant for stretching: If the centreline is not initially flat then under tension it will become so on a timescale much faster than that of stretching. Under compression, or negative tension, the sheet will buckle [1,5,6], again on a much faster timescale.
[2] The coefficient α_4 is always positive [8].

assuming that elastic effects are important at leading order. Since the director field is a 2D unit vector, we write it as

$$\boldsymbol{n} = (\sin\theta(x, z, t), 0, \cos\theta(x, z, t)). \tag{15}$$

We assume further that the elastic constants K_1 and K_3 are equal: $K_1 = K_3 = K$ (see e.g. [4, 17] for the validity of this commonly used assumption), and that any applied electric field has a leading-order component only in the z-direction:

$$\boldsymbol{E} = a(x)\boldsymbol{e}_z + O(\delta), \tag{16}$$

where $a(x)$ is determined in practice by the far field conditions on the externally applied electric field. A detailed justification of this field, which is the most general form compatible with Maxwell's equations and with no variation across the sheet, is given in Appendix A. We write $a(x) = E_a\tilde{a}(\tilde{x})$ to non-dimensionalise the electric field, where E_a is the alignment field strength introduced in (13).

With these scalings the normal $\boldsymbol{v} = \pm(0, 1) + O(\delta^2)$ so that condition (12) is indeed correct to order δ^2. Henceforth, we drop the tildes on the understanding that we are working in the dimensionless variables (unless explicitly stated otherwise).

2.2 Asymptotic expansion of the governing equations

We asymptotically expand all dependent variables (θ, u, v, p, h) in powers of $\delta = \hat{h}/L \ll 1$, and substitute into equations (1)–(3) to obtain a hierarchy of governing equations at orders 1, δ, δ^2 etc. The boundary conditions (9), (10) and (12) are Taylor-expanded onto the leading-order free boundaries $z = \pm h_0/2$ to yield conditions for the governing equations at each order in δ. In the dimensionless variables the bulk energy W in (7) is

$$W = \frac{1}{2}\left(\theta_z^2 + \delta^2\theta_x^2\right) - \delta e(x)\cos^2\theta - \delta\lambda e(x), \tag{17}$$

where

$$e(x) = \frac{\hat{h}LE_a^2 a(x)^2 \varepsilon(\varepsilon_\parallel - \varepsilon_\perp)}{K} = e_0 a(x)^2, \quad \lambda = \frac{\varepsilon_\perp}{\varepsilon_\parallel - \varepsilon_\perp}. \tag{18}$$

Here we suppose that $e(x)$ and λ are of order-one with respect to δ: since elasticity is present throughout the model, while the electric field may be zero or non-zero, we have scaled under the assumption that elasticity provides the dominant contribution to the bulk energy. The electric field, reflected by the presence of $e(x)$ in (17), then enters at first order in δ and is assumed comparable to the surface energy. These assumptions represent the smallest electric field that significantly affects the sheet. Larger field strengths so that $\delta e(x) = O(1)$ would lead to a different, more complicated model; yet larger fields would give total alignment of the director in the field, and a relatively simple system.

The x- and z-components of the momentum equation (2) and the energy equation (1) at leading order may now be written

$$u_{0zz}\left(2 - (\alpha_2 - \alpha_5)\cos^2\theta_0 + (\alpha_3 + \alpha_6)\sin^2\theta_0 + 2\alpha_1\sin^2\theta_0\cos^2\theta_0\right)$$
$$+ 2u_{0z}\theta_{0z}\left(\alpha_2 + \alpha_3 - \alpha_5 + \alpha_6 + 2\alpha_1\cos 2\theta_0\right)\sin\theta_0\cos\theta_0 = 0, \tag{19}$$

$$u_{0zz}\left(\alpha_1 + \alpha_2 + \alpha_3 + \alpha_5 + \alpha_6 + \alpha_1\cos 2\theta_0\right)\sin\theta_0\cos\theta_0 - 2\hat{N}\theta_{0zz}\theta_{0z}$$
$$+ u_{0z}\theta_{0z}\left(\alpha_1\cos 4\theta_0 + (\alpha_1 + \alpha_2 + \alpha_3 + 2\alpha_5)\cos 2\theta_0 - \alpha_2 + \alpha_3\right) = 0, \tag{20}$$

$$2\hat{N}\theta_{0zz} - u_{0z}\left(\alpha_2 - \alpha_3 + (\alpha_6 - \alpha_5)\cos 2\theta_0\right) = 0 \tag{21}$$

respectively, where the dimensionless inverse Ericksen number $\hat{N} = K/(\mu U\delta L)$ measures the relative importance of elastic and viscous effects. Note that with our chosen scalings, the dynamic coupling terms containing θ_t (arising from $\tilde{\mathbf{g}}$ in equations (1) and (2)) do not appear at this order: we have a quasi-static limit in which the director adapts 'instantaneously' to the changing geometry on the timescale of the axial fluid flow. The viscosities α_i in the above equations have all been scaled with $\mu = \alpha_4/2$ (hence, the non-dimensional $\alpha_4 \mapsto 2$). These equations must be solved subject to the leading-order boundary conditions at $z = \pm h_0/2$. The normal components of the stress conditions (9) at each interface yield, at order δ^{-1},

$$u_{0z} = 0 \quad \text{on } z = \pm h_0/2. \tag{22}$$

The leading order in the anchoring conditions (12) gives

$$\theta_0 = \theta_B g(a(x)) \quad \text{on } z = \pm h_0/2, \tag{23}$$

with g given by the dimensionless form of (13),

$$g(a) = \frac{1}{a^2 + 1}, \tag{24}$$

while the kinematic conditions (10) give

$$w_0 = \pm\frac{1}{2}(h_{0t} + u_0 h_{0x}) \quad \text{on } z = \pm h_0/2. \tag{25}$$

Eliminating u_{0z} between equations (20) and (21) reveals that θ_{0z} is constant and hence $u_{0z} = 0$. Applying the boundary conditions then determines

$$u_0 = u_0(x, t), \qquad \theta_0 = \theta_0(x) = \theta_B g(a(x)). \tag{26}$$

The incompressibility equation (3) may now be integrated at leading order to give an expression for w_0,

$$w_0 = -z u_{0x}, \tag{27}$$

where we have applied a kinematic condition (25) at the top surface. Applying the kinematic condition at the bottom surface provides the mass balance

$$h_{0t} + (u_0 h_0)_x = 0. \tag{28}$$

As with the Newtonian counterpart, at this stage there is no equation to specify u_0 and so we must examine higher orders in the governing equations. At order δ in the x- and z-components of (2) we find

$$u_{1zz} = 0, \tag{29}$$

$$p_{0z} = 0, \tag{30}$$

where (29) was used to obtain (30). Hence, $p_0 = p_0(x, t)$. The energy equation (1) at $O(\delta)$ gives

$$
\begin{aligned}
&u_{0x}(\alpha_5 - \alpha_6) \sin 2\theta_0 + \frac{1}{2}(\alpha_3 - \alpha_2 + (\alpha_5 - \alpha_6) \cos 2\theta_0) u_{1z} \\
&+ \hat{N}(\theta_{1zz} - e(x) \sin 2\theta_0) = 0.
\end{aligned}
\tag{31}
$$

This last equation will give θ_1 in terms of u_0, u_1 and θ_0.

We now require the boundary conditions at the appropriate order. The $O(1)$ normal component of the stress conditions (9) gives

$$
\begin{aligned}
u_{1z} &= \frac{u_{0x}(\alpha_6 - \alpha_5 + \alpha_1 \cos 2\theta_0) \sin 2\theta_0}{2 - (\alpha_2 - \alpha_5) \cos^2 \theta_0 + (\alpha_3 + \alpha_6) \sin^2 \theta_0 + 2\alpha_1 \sin^2 \theta_0 \cos^2 \theta_0} \\
&\equiv U_1(\theta_0) u_{0x},
\end{aligned}
\tag{32}
$$

on $z = \pm\frac{h_0}{2}$, where we use U_1 as convenient shorthand for the non-linear function of θ_0 on the right-hand side. Combining equations (29) and (32) gives

$$u_1 = z U_1(\theta_0) u_{0x} + U_0(x, t), \tag{33}$$

where U_0 is undetermined and U_1 is defined in (32). The $O(1)$ tangential components of the stress conditions (9) give the same result on both upper and lower free boundaries, $z = \pm h_0/2$,

$$
\begin{aligned}
p_0(x, t) &= -(2 + (\alpha_5 + \alpha_6 + \alpha_1 \cos 2\theta_0) \cos^2 \theta_0) u_{0x} \tag{34} \\
&+ \frac{u_{0x} U_1(\theta_0)}{2}(\alpha_1 + \alpha_2 + \alpha_3 + \alpha_5 + \alpha_6 + \alpha_1 \cos 2\theta_0) \sin \theta_0 \cos \theta_0 - \frac{\gamma}{2} h_{0xx} \\
&\equiv -f(\theta_0) u_{0x} - \frac{\gamma}{2} h_{0xx}, \tag{35}
\end{aligned}
$$

where $\gamma = \hat{\gamma}\delta/(\mu U)$ is a dimensionless surface tension coefficient and the function f is defined by (35) for later convenience. Since p_0 is known to be independent of z, (35) represents the leading-order pressure throughout the sheet.

We can now solve equation (31) for θ_1 after applying the appropriate anchoring conditions at $O(\delta)$, $\theta_1 = 0$ on $z = \pm h_0/2$. The problem reduces to

$$
\begin{aligned}
\theta_{1zz} &= e(x) \sin 2\theta_0 \tag{36} \\
&- \frac{u_{0x}}{\hat{N}}\left[(\alpha_5 - \alpha_6) \sin 2\theta_0 + \frac{U_1(\theta_0)}{2}(\alpha_3 - \alpha_2 + (\alpha_5 - \alpha_6) \cos 2\theta_0)\right] \\
&\equiv Q_1(x) \tag{37}
\end{aligned}
$$

(here $Q_1(x)$ is introduced as a convenient shorthand for the right-hand side of (36)). Hence, we determine the unique solution

$$\theta_1 = \frac{Q_1(x)}{2}\left(z^2 - \frac{h_0(x,t)^2}{4}\right). \tag{38}$$

We now have expressions for θ_0, θ_1, p_0 and a mass balance (28) relating the unknowns u_0, h_0. To close the system we must continue to yet higher orders. The algebra is too cumbersome to present in detail, so we merely outline the procedure: we examine equation (2) to $O(\delta^2)$, which leads to an equation for u_{2zz} of the form

$$u_{2zz} = \mathcal{K}(x,t),$$

where $\mathcal{K}$ has complicated dependence on $u_0(x,t), \theta_0(x,t)$. Integration across the sheet leads to

$$u_{2z}|_{z=h_0/2} - u_{2z}|_{z=-h_0/2} = h_0\mathcal{K}(x,t). \tag{39}$$

The boundary terms $u_{2z}|_{z=\pm h_0/2}$ are given in terms of u_0, h_0 by the stress conditions (9) at $O(\delta)$, leading to an equation relating u_0 and h_0. This equation together with (28) (and θ_0 given by (26)) forms a closed leading-order system.[3] In the most general case the new equation is far too lengthy (several pages) to reproduce profitably here; we discuss special cases separately below. Since we have now reduced the problem to one for leading-order dependent variables u_0, h_0, θ_0, we now drop the subscripts on these quantities.

2.2.1 *No electric field, $a(x) = 0 = e(x)$*

With no electric field, the leading order director angle θ is simply constant (see (26)), dictated by anchoring conditions: $\theta = \theta_B$. For general θ_B the solvability condition (39) takes the form

$$\frac{F(\theta_B)}{G(\theta_B)}\left(hu'(x)\right)_x + \frac{\gamma}{2}hh_{xxx} = 0, \tag{40}$$

where

$$G(\theta_B) = \alpha_1 - 2\alpha_2 + 2\alpha_3 + 8 + 2\alpha_5 + 2\alpha_6 - \alpha_1\cos(4\theta_B)$$
$$- 2\cos(2\theta_B)(\alpha_2 + \alpha_3 - \alpha_5 + \alpha_6),$$

$$F(\theta_B) = -\alpha_1\alpha_2 + \alpha_1\alpha_3 + 8\alpha_1 + 2\alpha_1\alpha_5 + 2\alpha_1\alpha_6$$
$$- 8\alpha_2 - \alpha_2\alpha_5 - 3\alpha_2\alpha_6 + 8\alpha_3 + 3\alpha_3\alpha_5 + \alpha_3\alpha_6$$
$$+ 32 + 16\alpha_5 + 16\alpha_6 + 2\alpha_5^2 + 4\alpha_5\alpha_6 + 2\alpha_6^2$$
$$- 2\cos(2\theta_B)(\alpha_1 + 4 + \alpha_5 + \alpha_6)(\alpha_2 + \alpha_3 - \alpha_5 + \alpha_6)$$
$$- \cos(4\theta_B)(\alpha_1(\alpha_2 - \alpha_3) + (\alpha_2 + \alpha_3)(\alpha_5 - \alpha_6)).$$

---

[3] A nice compact presentation of this process may be found in the appendix of [7] for the poroviscous sheet model.

Although $F(\theta_B)$ and $G(\theta_B)$ take complicated forms, they are just constants for a fixed anchoring angle θ_B, and we lose no generality by setting $\theta_B = 0$ in the analysis. We then obtain

$$(4 + \alpha_1 + \alpha_5 + \alpha_6)(u_x h)_x + \frac{\gamma}{2} h h_{xxx} = 0, \tag{41}$$

which must be solved together with equation (28),

$$h_t + (uh)_x = 0. \tag{42}$$

The governing equations for a Newtonian film are retrieved by setting $\alpha_1 = \alpha_2 = \alpha_3 = \alpha_5 = \alpha_6 = 0$. In general then, the above equations are equivalent to the Newtonian case, with a only difference of surface tension coefficient. The first term in (41) is the axial gradient of the (leading-order) dimensionless tension in the sheet, and the pre-multiplying factor is known as the Trouton ratio. The Newtonian limit of equations (41) and (42) with zero surface tension, $\gamma = 0$, is known as the Trouton model for a viscous sheet, and was considered in detail by Howell [5, 6] (see also references therein for earlier work on similar systems).

Appropriate boundary and initial conditions for equations (41) and (42) are that the initial profile of the sheet, $h_i(x) = h(x, 0)$, is specified, and that we apply conditions at each end of the sheet. We consider a sheet stretched between two plates that are pulled apart. We assume that one plate (one end of the sheet) is fixed: $u(0, t) = 0$, while the other, at $x = s(t)$, is pulled either with (a) prescribed velocity, or (b) prescribed force F. In case (a) the appropriate condition is $u(s(t), t) = \dot{s}(t)$, with $s(t)$ given; and in case (b) we have $F = h(s(t), t)(-p(s(t), t) + 2u_x(s(t), t))$, where F is prescribed but $s(t)$ is unknown. (In this latter case (b) no liquid crystal-specific behaviour is apparent in the force balance; this is a consequence of the fact that $\theta_z = 0$ to leading order.) With $\gamma = 0$, these conditions suffice to close the problem; but if $\gamma \neq 0$ then we need an extra condition at each end, such as specification of the contact angle $\partial h / \partial x$ between the fluid and the plate. The boundary conditions are discussed further when solutions are presented in Section 3.

Since, to this order in the asymptotics, the electric field-free case is equivalent to the Newtonian one, which was considered exhaustively by Howell and co-authors [5, 6], we move on to a more complex model that results when an electric field is applied.

2.2.2 *Applied electric field*

The analogue of equation (41) is extremely complicated with an applied field (several pages of Mathematica output), and in the most general case it is not clear whether it can be simplified significantly. However, since with no applied field we obtained the Newtonian result (modulo a rescaling of surface tension), we are encouraged here also to examine the special case $\alpha_1 = \alpha_2 = \alpha_3 = \alpha_5 = \alpha_6 = 0$ to make further progress. The nematic character is explicitly retained in the elastic energy, and in the way the fluid responds to the applied field. This approximation probably gives a reasonable description of the response of a nematic to an applied field when near its isotropic transition.

The appropriate governing equation is then equation (42):

$$h_t + (uh)_x = 0 \tag{43}$$

and, from the solvability condition (39),

$$4(u_x h)_x + \hat{N} h (e(x)(\cos^2 \theta + \lambda))_x + \frac{\gamma}{2} h h_{xxx} = 0, \tag{44}$$

where $e(x)$ and λ are as defined in (18),

$$e(x) = \frac{\hat{h} L E_a^2 a(x)^2 \varepsilon (\varepsilon_\| - \varepsilon_\perp)}{K} = e_0 a(x)^2, \quad \lambda = \frac{\varepsilon_\perp}{\varepsilon_\| - \varepsilon_\perp}, \tag{45}$$

and the director angle θ is prescribed by (26b) and (24),

$$\theta_0(x) = \theta_B g(a(x)), \quad \text{with} \quad g(a) = \frac{1}{a^2 + 1}, \tag{46}$$

where θ_B is the constant anchoring angle. The function $a(x)$ is determined by knowledge of the externally applied electric field; see Appendix A. In Appendix A we outline a procedure for calculating the electrode shape required to generate a given choice of $a(x)$, and therefore we consider $a(x)$ to be a prescribed function in the model. The problem then reduces to solving (43)–(46) for u, h, subject to appropriate boundary conditions as outlined in Section 2.2.1. In the following sections we consider various approaches to solving this model.

3 Simple model solutions

We first consider some simple exact solutions of our models (43)–(46): (i) steady state, achievable (in a non-trivial sense) only for the fixed-force end condition and with non-zero surface tension γ; and (ii) exact unsteady 'pulling' solutions, where the end velocity is prescribed, but surface tension is zero. These solutions, which we present only for simple choices of electric field, can act as a guide for more general numerical solutions, which we present in Section 4.

We note that, for the steady solutions considered below, and for our subsequent numerical results, it is convenient to work on a fixed length domain $[0, 1]$. We therefore rescale by choosing $\xi = x/s(t)$, where $x = s(t)$ denotes the right-hand end of the sheet. Then the governing equations are

$$4s(u_\xi h)_\xi + \hat{N} h s^2 \left[e(\xi)(\cos^2 \theta + \lambda) \right]_\xi + \frac{\gamma}{2} h h_{\xi\xi\xi} = 0, \tag{47}$$

$$s h_t - \xi s_t h_\xi + (uh)_\xi = 0 \tag{48}$$

together with (45), and our definition (46) for θ.

Specified end velocity: When the velocities of the sheet ends are specified, appropriate boundary and initial conditions are

$$u(0, t) = 0, \qquad u(1, t) = s_t(t), \qquad h(\xi, 0) = h_i(\xi), \tag{49}$$

$$h_\xi(0, t) = -s\beta_0, \qquad h_\xi(1, t) = s\beta_1, \tag{50}$$

where $s(t)$ is prescribed (and $s(0) = 1$), and β_0, β_1 are related to the contact angles ϕ_0, ϕ_1 at $x = 0$, $x = s(t)$ respectively (the appropriateness of these contact angle

boundary conditions (50) is discussed further in Appendix B). Within the level of approximation already carried out, we may write $\phi_j = \pi/2 - \delta\beta_j$. These angles β_0, β_1 are specified when $\gamma \neq 0$; if surface tension is neglected we require only the first set of conditions (49).

Specified pulling force: If motion is driven by a specified force applied at one end of the bridge, an extra condition is required, since the domain length $s(t)$ in x-space (the sheet length) is unknown. This condition is an explicit conservation of mass constraint, which was automatically enforced by the previous boundary conditions (49). The force condition at the pulling end is

$$F = h(-p + 2u_x) \quad \text{at } x = s(t), \tag{51}$$

and thus the boundary conditions (49) are replaced by

$$u(0,t) = 0, \quad F = h\left[\frac{f(\theta)}{s}u_\xi + \frac{\gamma}{2s^2}h_{\xi\xi} + \frac{2}{s}u_\xi\right]_{\xi=1}, \tag{52}$$

$$V = s\int_0^1 h\,d\xi, \tag{53}$$

where $f(\theta)$ is as defined in (35). The position of the right-hand boundary is defined by

$$s_t = u(1,t), \quad s(0) = 1. \tag{54}$$

Conditions (50) still hold if $\gamma \neq 0$.

3.1 Steady states

With a prescribed (non-zero) velocity at the ends there is clearly no steady state; however, with a prescribed force a steady state is possible. In this case the mass balance (48) shows that uh is constant, and since $u(0,t) = 0$, we infer that $u = 0$ everywhere. Setting $u = 0$ in (47), h is then determined by

$$\hat{N}s^2\left[e(\xi)(\cos^2\theta + \lambda)\right]_\xi + \frac{\gamma}{2}h_{\xi\xi\xi} = 0. \tag{55}$$

With no field the film thickness is quadratic, with coefficients fixed by conditions (50) and (52),

$$h = \frac{s}{2}(\beta_1 + \beta_0)\xi^2 - s\beta_0\xi + \frac{2sF}{\gamma(\beta_0 + \beta_1)} + \frac{s}{2}(\beta_0 - \beta_1). \tag{56}$$

If $F = 0$, we note that $h(1,t) = 0$ (so the bridge vanishes at the end) indicating the existence of a minimum force condition. In fact, expression (56) does not even guarantee a non-negative film thickness, so solutions must be checked for this property as well as for positive sheet length. For example, when $\beta_1 > 0$, to ensure $h > 0$ requires $F > \gamma\beta_1^2/4$.

The sheet length s is determined by the volume constraint (53) as

$$s^2 = V \left[\frac{2F}{\gamma(\beta_0 + \beta_1)} + \frac{1}{6}(\beta_0 - 2\beta_1) \right]^{-1}. \tag{57}$$

This relation shows that s decreases as F increases, that is, a greater force results in a shorter bridge. This seemingly counter-intuitive result is explained by the fact that a short, highly curved bridge can resist a greater pulling force: a longer, less curved bridge can only balance a lesser force. A sufficiently large force applied to a short bridge would indeed elongate it, but if the force were sustained at the same high level, then the bridge would elongate indefinitely and no steady state could be achieved. Due to the requirement that $s^2 > 0$, equation (57) leads to

$$F > \frac{\gamma(2\beta_1 - \beta_0)(\beta_0 + \beta_1)}{12}. \tag{58}$$

This is the minimum force required to balance surface tension in the steady state (but we must also ensure that the force is sufficient that $h > 0$).

With an electric field equation (55) integrates once immediately, but then the remaining integration depends on the form of the field. In the simplest non-trivial case, where the term $\left[e(x)(\cos^2 \theta + \lambda) \right]$ is linear in x,

$$E_F = \hat{N} \left[e(x)(\cos^2 \theta + \lambda) \right]_x, \tag{59}$$

for constant E_F, then

$$h = -\frac{E_F s^3 \xi^3}{3\gamma} + \left[(\beta_0 + \beta_1) + \frac{s^2 E_F}{\gamma} \right] \frac{s\xi^2}{2} - \beta_0 s\xi + \frac{2sF}{\gamma(\beta_0 + \beta_1) - s^2 E_F}$$
$$- \frac{s^3 E_F}{6\gamma} + \frac{s}{2}(\beta_0 - \beta_1). \tag{60}$$

Such an electric field can be generated by suitably shaped converging electrodes, as outlined in Appendix A. Again, $h(1, t) = 0$ when $F = 0$, so the electric field alone cannot balance surface tension and a minimum force must still be applied. The position s of the sheet's end is again determined by (53), which leads to a cubic equation for $y = s^2$:

$$(E_F y - \gamma(\beta_0 + \beta_1)) \left[V - \frac{y}{12} \left(2(\beta_0 - 2\beta_1) - \frac{E_F y}{\gamma} \right) \right] + 2Fy = 0. \tag{61}$$

The requirement that $y > 0$ for a given field E_F restricts the possible values for F; or *vice versa* if one thinks of specifying F and finding the field E_F that gives a steady solution.

We may obtain approximate solutions for h and s in the limit $E_F \gg 1$ (note E_F must be positive), with $F \sim O(1)$. In this case an asymptotic expansion on the small parameter E_F^{-1} can be constructed,

$$s^2 = \frac{\gamma(\beta_0 + \beta_1)}{E_F} \left[1 - \frac{2F}{V E_F} + O\left(\frac{1}{E_F^2} \right) \right],$$
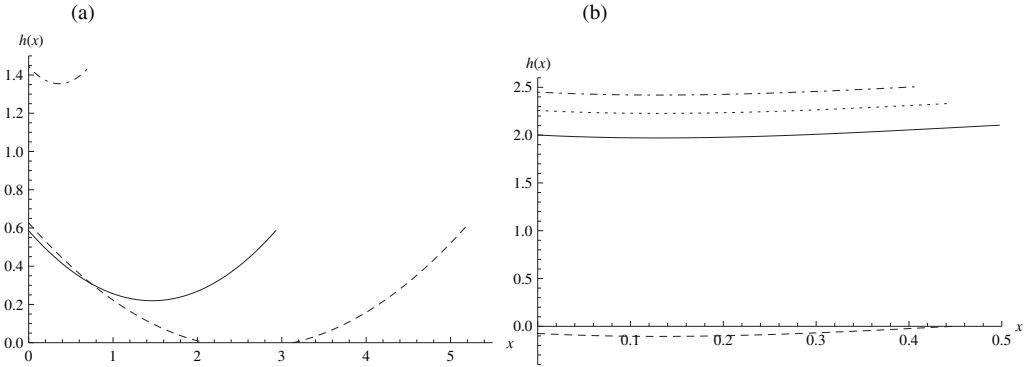
FIGURE 2. Steady-state solutions with (a) $E_F = 0$ and $F = 0.06$ (dashed; negative over part of domain), 0.1 (solid), 1 (dot-dashed); (b) $E_F = 5$ and $F = 0$ (dashed; nowhere positive), -0.5 (solid), 0.05 (dotted), 0.5 (dot-dashed).

while the thickness may be written as

$$
\begin{aligned}
h = {} & \frac{V}{\sqrt{\gamma(\beta_0 + \beta_1)}} E_F^{1/2} \\
& + \left[\frac{-(\beta_0 + \beta_1)\xi^3 + 3(\beta_0 + \beta_1)\xi^2 - 3\beta_0\xi - (2\beta_1 - \beta_0) - 3F}{3\sqrt{\gamma(\beta_0 + \beta_1)}} \right] E_F^{-1/2} \\
& + O\left(E_F^{-3/2}\right).
\end{aligned}
$$

This solution is valid for both extensional and compressive forces F as long as $|F| \ll E_F$.

If the applied force F is large (with $E_F \sim O(1)$) then we require $F > 0$ for solutions to exist. We may easily write down an approximate solution for $y = s^2$ in terms of the small parameter F^{-1},

$$
s^2 = \frac{\gamma V}{2F}(\beta_0 + \beta_1) \left[1 - \frac{1}{12F}\left(\gamma(\beta_0 + \beta_1)(\beta_0 - 2\beta_1) + 6E_F V\right) + O\left(\frac{1}{F^2}\right) \right].
$$

This solution is valid for fields E_F of either sign as long as $|E_F| \ll F$. As with the large F expansion when $E_F = 0$, the film is short and fat and at leading order the thickness is constant with the curvature appearing only at order $F^{-3/2}$,

$$
h = \sqrt{\frac{2V}{\gamma(\beta_0 + \beta_1)}} F^{1/2} \left(1 + \frac{6E_F V - \gamma(\beta_0 + \beta_1)(\beta_0 - 2\beta_1)}{24} F^{-1} + O(F^{-2}) \right).
$$

Several solutions, which illustrate a range of possibilities, are shown in Figure 2. In all cases $\beta_0 = \beta_1 = 0.5$, which gives positive curvature, and $\gamma = 1 = V$. Figure 2(a) shows the case where $E_F = 0$. The bottom curve, with $F = 0.06$, does not satisfy the condition $F > \gamma\beta_1^2/4 = 0.0625$ and leads to a negative thickness over part of the domain. The other two curves do satisfy this condition and show clearly how, as F increases, the thickness also increases while the length s decreases. Figure 2(b) shows solutions with a

non-zero field, $E_F = 5$. Increasing F leads to shorter and fatter bridges. Also shown is a non-physical solution where $F = 0$ and the height is everywhere negative.

A negative value for E_F augments the surface tension force and so allows longer bridges; a positive value gives shorter bridges. If we choose $\beta_0 = \beta_1 < 0$, there is no real solution for s; no steady state of this kind exists, and presumably this form of bridge would rupture, likely at its end(s).

3.2 Solution of the zero surface tension model, $\gamma = 0$

We now consider the case in which surface tension is negligible, setting $\gamma = 0$ in the model (43)–(46) summarised in Section 2.2.2. Following the approach of Howell [5, 6] for Newtonian sheets, this model may be solved by introducing a Lagrangian transformation $(x, t) \mapsto (\eta, \tau)$, where

$$x_\tau = u(x(\eta, \tau), \tau), \quad x(\eta, 0) = \eta, \quad t = \tau. \tag{62}$$

Then

$$\partial_\tau = \partial_t + u \partial_x, \quad \text{and} \quad u_\eta = u_x x_\eta,$$

so that (42) becomes

$$h_\tau + \frac{h u_\eta}{x_\eta} = 0. \tag{63}$$

Now note that $u = x_\tau$, so $u_\eta = x_{\eta\tau}$, and (63) becomes

$$h_\tau x_\eta + h x_{\eta\tau} = (h x_\eta)_\tau = 0 \quad \Rightarrow \quad x_\eta = \frac{h_i(\eta)}{h(\eta, \tau)}, \tag{64}$$

where $h_i(\eta) = h(\eta, 0)$ is the initial condition on the sheet profile.

In equation (44) we write

$$R(x) = \left(e(x)(\cos^2 \theta + \lambda) \right)_x. \tag{65}$$

In line with our approach in the previous section, we consider $R(x)$ to be a specifiable function ($e(x) = e_0 a(x)^2$, $\theta = g(a(x))$ is a given function of $a(x)$, and as described in Appendix A, we can propose a method to calculate the electrode shape required to generate any given $a(x)$). Writing the first term in (44) as $-4(h_\tau)_x$, and using (64), equation (44) (with $\gamma = 0$) becomes

$$\frac{4 h_{\eta\tau}}{x_\eta} = \hat{N} R h \quad \Rightarrow \quad 4 h_{\eta\tau} = \hat{N} R h_i, \tag{66}$$

where R is defined in (65). The system is closed by suitable boundary conditions as already discussed; with zero surface tension it is sufficient to specify the positions of the sheet's ends, or fix one end and specify the force applied to the other end. In the former case it

is easy to integrate twice to find the explicit solution parametrically:

$$h(\eta, \tau) = A(\tau) + h_i(\eta) + \frac{\tau \hat{N}}{4} \int_0^\eta R(\eta', \tau) h_i(\eta') \, d\eta', \tag{67}$$

where h_i is the initial condition on the sheet thickness, $h(\eta, 0) = h_i(\eta)$ and $A(\tau)$ is fixed by specifying the sheet length $s(\tau)$, with $A(0) = 0$:

$$s(\tau) = \int_0^1 x_\eta \, d\eta = \int_0^1 \frac{h_i(\eta) \, d\eta}{A(\tau) + h_i(\eta) + \frac{\tau \hat{N}}{4} \int_0^\eta R(\eta', \tau) h_i(\eta') d\eta'}. \tag{68}$$

For physically relevant solutions we assume $s(\tau)$ is a prescribed, increasing function of τ, with $s(0) = 1$.

The latter condition of a prescribed force at the sheet's end leads to a more complicated free boundary problem, and the exact solution cannot be obtained so neatly. We do not consider this case further analytically.

3.2.1 *Specific solution family: Rh_i constant*

The simplest non-trivial case to consider is when the combination Rh_i is constant (e.g. constant R, as considered for the solutions in Section 3.1, and an initially flat sheet). Since $h_i > 0$ necessarily, R is then of one sign for all relevant η, so with no loss of generality we write $R(\eta)h_i(\eta) = \text{sgn}(R)$, and explicitly evaluate the integral in (67) to give

$$h(\eta, \tau) = A(\tau) + h_i(\eta) + \text{sgn}(R)\frac{\hat{N}\eta\tau}{4}. \tag{69}$$

To determine $A(\tau)$ then requires that we evaluate the integral in (68),

$$s(\tau) = \int_0^1 \frac{h_i(\eta) \, d\eta}{A(\tau) + h_i(\eta) + \text{sgn}(R)\frac{\hat{N}\eta\tau}{4}} = \int_0^1 \frac{d\eta}{1 + |R|\left(A(\tau) + \text{sgn}(R)\frac{\hat{N}\eta\tau}{4}\right)}, \tag{70}$$

which requires specification of h_i or R, and the pulling function $s(\tau)$.

For a particular case in which both h_i and R are constant ($h_i(\eta) = 1$, $R(\eta) = \text{sgn}(R)$) we can evaluate $A(\tau)$ explicitly, and also invert relation (64) to find $x(\eta, \tau)$, obtaining the exact solution parametrically as

$$h(\eta, \tau) = \frac{\text{sgn}(R)\hat{N}\eta\tau}{4} + \frac{\text{sgn}(R)\hat{N}\tau}{4(\exp(\frac{\text{sgn}(R)\hat{N}\tau}{4}s(\tau)) - 1)}, \tag{71}$$

$$x(\eta, \tau) = \frac{4}{\text{sgn}(R)\hat{N}\tau} \log\left[\eta\left(\exp\left(\frac{\text{sgn}(R)\hat{N}\tau}{4}s(\tau)\right) - 1\right) + 1\right], \tag{72}$$

for $\eta \in [0, 1]$, $\tau > 0$. For any monotone increasing pulling function $s(\tau)$ (assuming $s(\tau) < \infty$ while $\tau < \infty$) these solutions thin indefinitely at the ends (for both $\text{sgn}(R) > 0, < 0$), but do not break off in finite time. Typical solutions for constant pulling speed are shown in Figures 3 and 4.
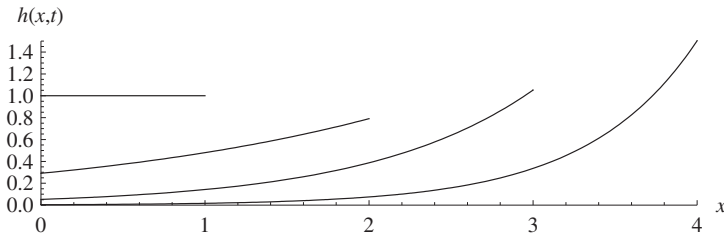
FIGURE 3. Exact solution to the unsteady problem for an initially uniform sheet $h(x, 0) = h_i(x) = 1$, with the right-hand end pulled at unit speed so that its position is at $s(t) = 1 + t$. The sheet profile is shown at times $t = 0, 1, 2, 3$. The applied field is such that $R(x) = 1$ (as defined in (65)), and the parameter $\hat{N} = 2$.
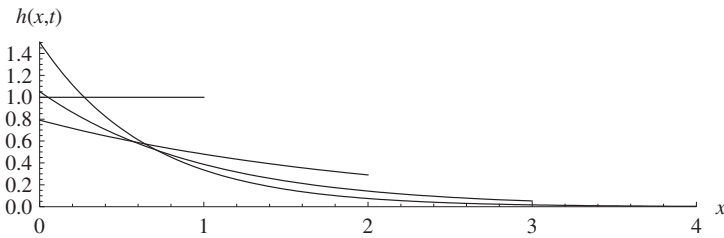

FIGURE 4. As for Figure 3, but with $R(x) = -1$.

The case $R(x) = 1$ (Figure 3) corresponds (in qualitative terms) to an electric field increasing along the positive x-axis. This induces a flux of fluid along the positive x-direction so that it piles up at the right-hand end of the sheet, while the left-hand end thins. For $R(x) = -1$ the opposite is true: the electric field decreases along the positive x-direction, and the induced flux is in the opposite direction. By way of contrast we note that the equivalent Newtonian solution for $h_i(\eta) = 1$ is simply

$$h(\eta, \tau) = \frac{1}{s(\tau)}, \quad x = \eta s(\tau) \tag{73}$$

(set $\hat{N} = 0$ in (67), (68) and (64)), so the Newtonian sheet simply thins uniformly to conserve mass.

In Figures 5 and 6 we show analogous solutions of (64), (69) and (70) for an initially quadratic sheet profile $h(x, 0) = h_i(x) = 1/2 + (x - 1/2)^2$ pulled at unit speed from the right-hand end ($s(t) = 1 + t$). Note that although the sheet is initially thinnest at the point mid-way between its ends, this is not the case after significant stretching: the flux induced by the electric field gradient dominates in both cases, and by time $t = 5$ the sheet is thinnest at one of its ends.

The question of sheet breakup, whether internal or at an endpoint, is non-trivial to address. Equations (64) and (68) show that the length of a general zero-surface tension sheet satisfies

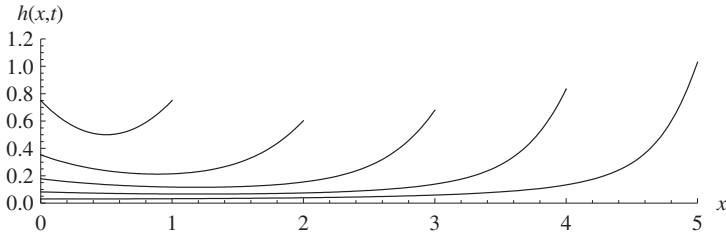$$s(\tau) = \int_0^1 \frac{h_i(\eta)}{h(\eta, \tau)} d\eta.$$

FIGURE 5. Exact solution to the unsteady problem for an initially quadratic sheet $h(x,0) = h_i(x) = 1/2 + (x - 1/2)^2$, with the right-hand end pulled at unit speed so that its position is at $s(t) = 1 + t$. The sheet profile is shown at times $t = 0, 1, 2, 3, 4$. The applied field is such that $R(x)h_i(x) = 1$ (R is as defined in (65)), and the parameter $\hat{N} = 1$.
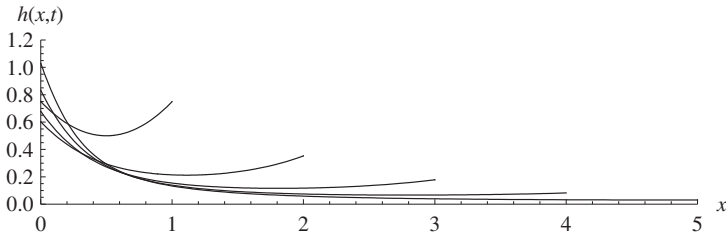

FIGURE 6. As for Figure 5, but with $R(x)h_i(x) = -1$.

For a non-zero initial profile $h_i(\eta) > 0$, if $h(\eta^*, \tau^*) = 0$, $1/h$ must be integrable in the neighbourhood of η^*, suggesting that if a profile goes to zero in finite time, it may do so with local cusp-type behaviour $h \sim |\eta - \eta^*|^\alpha$, $0 < \alpha < 1$, rather than smoothly. Whether such breakup can occur or not remains an open question mathematically: from a modelling perspective, our lubrication scaling assumptions would be violated before such cusp formation was achieved, in any case.

So far in our simulations with this solution family, the film is always ultimately thinnest at one of its ends, and so presumably breaks there first in practice, as the above examples suggest.

4 Numerical solutions of the full model

We now present some numerical solutions of the full (time-dependent, non-zero surface tension) model equations (47)–(48).

The first example that we consider is the non-zero surface tension analogue of the exact solution of Section 3.2.1. Again, we take the electric field to be such that $R(x) = \pm 1$, as defined in (65), and fix one end $x = 0$ of the initially uniform sheet ($h_i(x) = 1$), while the other end at $x = s(t)$ is pulled at unit speed so that $u(s(t), t) = 1$, with $s(t) = 1 + t$ (c.f. (49)). This form of electric field is particularly simple to implement, since the governing equation (47) reduces to

$$4s(u_\xi h)_\xi \pm \hat{N} h s^3 + \frac{\gamma}{2} h h_{\xi\xi\xi} = 0. \tag{74}$$

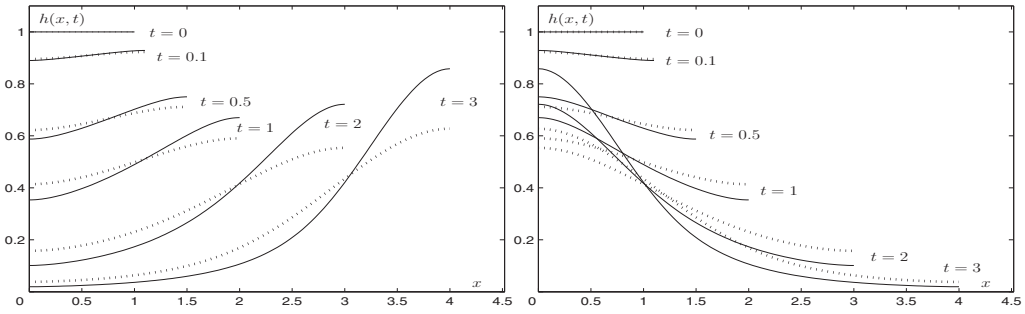Since we include surface tension effects, we must also specify the contact angles at

FIGURE 7. Numerical solutions to the unsteady problem with non-zero surface tension for an initially uniform sheet $h_i(x, 0) = 1$, with left-hand end fixed at $x = 0$ and right-hand end fixed at $s(t) = 1 + t$ (pulled at unit speed). The applied field is such that $R(x)$ (defined in (65)) takes values $R(x) = 1$ (left-hand figure) and $R(x) = -1$ (right-hand figure); and $\hat{N} = 2$ in both cases. The sheet profile $h(x, t)$ is shown at times $t = 0, 0.1, 0.5, 1, 2, 3$ for surface tension $\gamma = 2$ (solid) and $\gamma = 8$ (dashed).
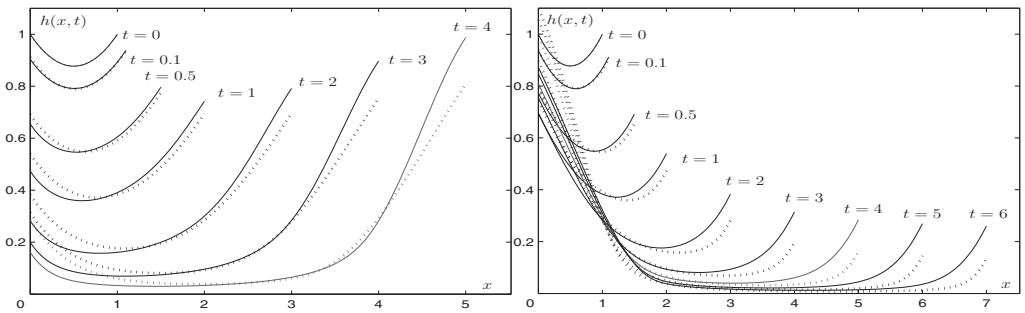
FIGURE 8. Evolution of a non-flat initial sheet (75) under the action of the electric field such that $R(x) = 1$ (left-hand plot; profile $h(x, t)$ shown at times $t = 0, 0.1, 0.5, 1, 2, 3, 4$) and $R(x) = -1$ (right-hand plot; profile $h(x, t)$ shown at times $t = 0, 0.1, 0.5, 1, 2, 3, 4, 5, 6$). Other details are as for Figure 7.

the sheet's ends, as in (50). For an initially flat sheet we choose contact angles of $\pi/2$ ($\beta_0 = 0 = \beta_1$) compatible with the initial condition. The resulting numerical solutions are shown in Figure 7, in which the left-hand figure with $R(x) = 1$ may be directly compared with Figure 3, and the right-hand figure with $R(x) = -1$ may be compared with Figure 4. The parameter $\hat{N} = 2$ in both cases, and results for surface tension parameter values $\gamma = 2$ (solid curves) and $\gamma = 8$ (dashed curves) are shown. The sheet profile is shown at times $t = 0.1, 0.5, 1, 2, 3$ as it extends.

Different contact angles are illustrated by means of a different initial condition,

$$h_i(\xi, 0) = c \cosh([\xi - 0.5]/c) - c \cosh(0.5/c) + 1, \tag{75}$$

with $c = 1.039$ to match boundary conditions (50) with contact angle parameters $\beta_0 = \beta_1 = 0.5$. Simulations for this initial condition are shown in Figure 8 (the left-hand sub-figure has $R(x) = 1$, while $R(x) = -1$ in the right-hand sub-figure). The sheet's right-hand end is pulled at unit speed, the parameter $\hat{N} = 2$, and results for two surface tension values
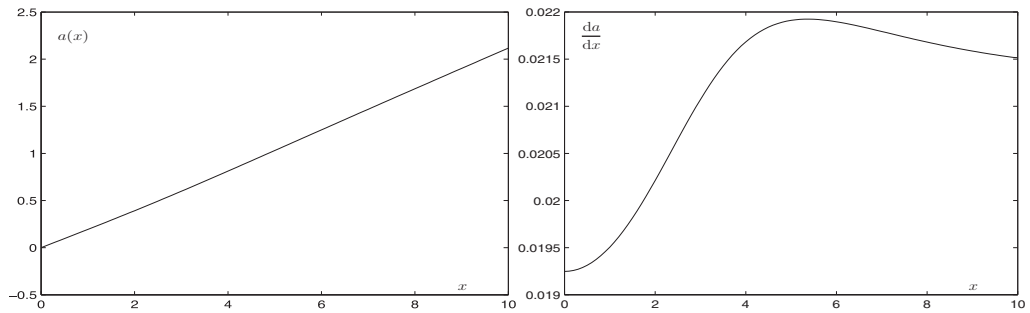
FIGURE 9. Electric field function $a(x)$ and its derivative for the external field (76).

$\gamma = 2$ (solid curves) and $\gamma = 8$ (dashed curves) are shown. The evolution is shown over longer times here to give a sense of the large-time evolution of such a sheet. While the behaviour is qualitatively similar in zero and non-zero surface tension cases, the general feature observed is that the sheet thins more rapidly as surface tension decreases. These observations suggest that non-zero surface tension will delay breakup (although in none of our simulations does breakup occur).

The final example that we consider illustrates a case in which instead of specifying $a(x)$, we specify the externally applied electric field, $\boldsymbol{E}_{\text{ext}}$, across an initially uniform sheet. We use the external field given as an example in (A 5) (Appendix A),

$$\boldsymbol{E}_{\text{ext}} = \hat{z}\boldsymbol{e}_x + x\boldsymbol{e}_{\hat{z}}, \tag{76}$$

where $\hat{z}$ is related to the dimensionless coordinate z (used from Section 2.2 onwards) by $\hat{z} = \delta z$ (it is the dimensionless but unstretched coordinate perpendicular to the sheet). The corresponding field within the sheet is

$$\boldsymbol{E} = a(x)\boldsymbol{e}_z + O(\delta), \tag{77}$$

where $a(x)$ is determined by solving equation (A 6) numerically in Appendix A. The function $a(x)$, together with its gradient, is shown in Figure 9; it is very close to linear.

This function $a(x)$ is substituted in (47), which is then solved together with (48) subject to the boundary conditions. The results for the sheet evolution are shown in Figures 10 (end velocity of sheet specified) and 11 (constant force prescribed at the sheet's end) for the two surface tension values, $\gamma = 2$ and $\gamma = 8$.

5 Discussion and conclusions

We have used systematic asymptotic expansions to derive a new model for the dynamics of a thin film of NLC, under the action of stretching from its ends, and an externally applied electric field. With certain simplifying assumptions (as outlined in Section 2), we deduce that, as for the Newtonian case, the sheet is flat to leading order, its centreline lying along the x-axis. The asymptotic analysis must be taken to second order in the film aspect ratio in order to obtain a closed system; when this is done, two coupled partial differential equations are obtained for the sheet thickness $h(x, t)$, and the velocity of the
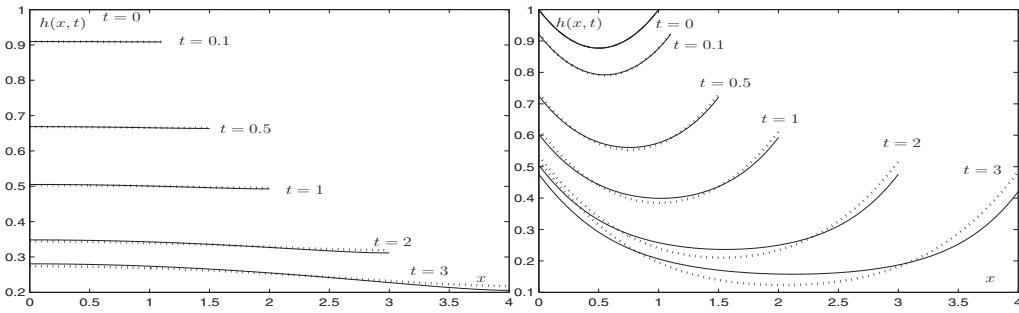
FIGURE 10. Numerical solutions to the unsteady problem with non-zero surface tension for an initially uniform sheet $h_i(x,0) = 1$ (left-hand figure) and non-flat initial condition (75) (right-hand figure). The left-hand end is fixed and its right-hand end is pulled at unit speed so that its position is at $s(t) = 1 + t$. The applied field is given by (76) and (77) ($a(x)$ as defined in (A 6) and plotted in Figure 9). The sheet profile $h(x,t)$ at times $t = 0, 0.1, 0.5, 1, 2, 3$ is shown for surface tension $\gamma = 2$ (solid) and $\gamma = 8$ (dashed).
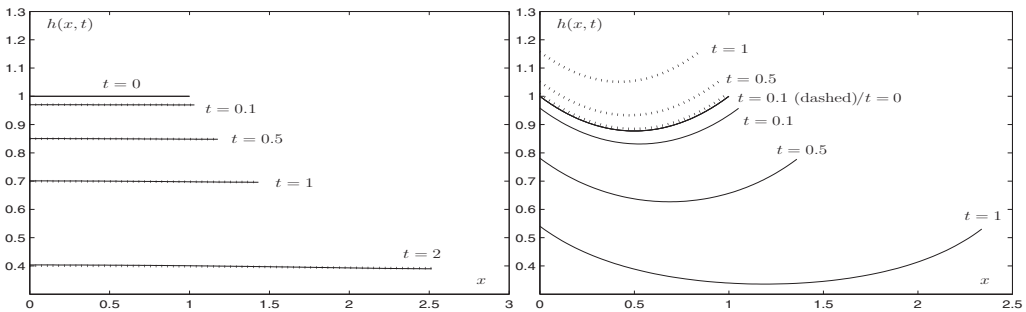

FIGURE 11. Numerical solutions to the unsteady problem with non-zero surface tension for an initially uniform sheet $h_i(x,0) = 1$ (left-hand figure, sheet profile shown at times $t = 0, 0.1, 0.5, 1, 2$) and non-flat initial condition (75) (right-hand figure, sheet profile shown at times $t = 0, 0.1, 0.5, 1$). The left-hand end is fixed, while the right-hand end is pulled with a force of 1.8 units, and the applied field is as for Figure 10. Surface tension values $\gamma = 2$ (solid) and $\gamma = 8$ (dashed) are shown.

sheet along its axis, $u(x,t)$. These partial differential equations depend also on the director angle θ, which, with the same anchoring conditions on each free surface, is also a function only of the axial coordinate (and possibly time), $\theta(x,t)$. This anchoring angle in turn is determined by the anchoring conditions at the free surfaces of the sheet and by the externally applied electric field, which can be solved separately as explained in Appendix A. The method for calculating the electric field is another contribution of this paper.

The full system, accounting for surface tension effects, the applied field, the surface anchoring of the nematic molecules and suitable conditions at the sheet's ends, is summarized in Section 2.2.2. With no applied field, it is found that the evolution is exactly as for a Newtonian sheet, but the presence of an electric field gradient can change matters dramatically. An exact method for finding solutions (which follows the approach of Howell [5] for the Newtonian case) is presented for the case of zero surface tension. When surface tension effects are significant, numerical methods must be used, and several examples are presented for this case.

The analysis has several limitations, which require a more in-depth (and considerably more complicated) analysis to resolve. Firstly, in order to solve explicitly for the director angle, we consider only electric field effects that are subdominant to the internal elasticity of the sheet (although they can dominate over surface anchoring effects). Therefore, our analysis will be valid only for moderate applied electric fields. Secondly, motivated in part by our zero-field results, which reduced to the Trouton model for the Newtonian sheet, we used a 'Newtonian' simplification to reduce the governing equations in the applied-field case: that is, we set all the Leslie viscosities other than the Newtonian analogue, $\alpha_4/2$ (unity in the dimensionless variables) to zero. While this simplification is rigorously justifiable in the field-free case, it is not obvious whether it is legitimate in the more general case with an applied field: likely, it is a reasonable description of the behaviour only near the nematic-isotropic transition. This issue would benefit from further consideration, and in a future publication we will investigate some very simple flows with an applied field and different (non-zero) Leslie viscosities.

Experiments on a similar setup (but with liquid crystalline fibres, rather than sheets, in extensional flow) have been carried out by Savage *et al.* [15]. Although Newtonian fibres in extension are governed by the same model as Newtonian sheets in extension (with a change only of Trouton ratio; the model is the same as the field-free case derived here), an extensional nematic fibre is quite different to an extensional nematic sheet, primarily because of surface anchoring. With a nematic sheet, it is trivial for the director to adopt the same anchoring condition on each free surface (uniform director field throughout the sheet). However, for a circular fibre, any non-planar anchoring at the fibre surface leads to a non-trivial problem for the equilibrium director field within the fibre. Thus, the asymptotic analysis for an extensional nematic fibre will be much more complicated in general than the sheet considered here. These differences make it impossible to compare our results with those of [15].

Appendix A The electric field within the sheet

The applied field satisfies Maxwell's equations both inside and outside the nematic sheet, with appropriate jump conditions at the interfaces. Within the sheet the slender scalings apply, with $x \sim L$, $z \sim \delta L$; and if $|\boldsymbol{E}| \sim E_0$ then the electric potential $\Psi \sim \delta L E_0$. In

dimensionless variables with these scalings, then the electric field within the sheet satisfies

$$\boldsymbol{E} = \nabla\Psi = \delta\Psi_x\boldsymbol{e}_x + \Psi_z\boldsymbol{e}_z \qquad (A\,1)$$

(in order to avoid a profusion of minus signs, we opt for this definition rather than the more usual $\boldsymbol{E} = -\nabla V$). Accounting for the dielectric anisotropy within the nematic, Maxwell's equations require $\nabla \cdot (\underline{\underline{\varepsilon}}\boldsymbol{E}) = 0$, so that

$$(\varepsilon_{33}\Psi_z)_z + \delta(\varepsilon_{13}\Psi_x)_z + \delta(\varepsilon_{13}\Psi_z)_x + \delta^2(\varepsilon_{11}\Psi_x)_x = 0$$

within the sheet. In this 2D case the coefficients of the dielectric tensor $\underline{\underline{\varepsilon}}$ can be written explicitly in terms of the director components $n_1 = \sin\theta$ and $n_3 = \cos\theta$, as

$$\varepsilon_{33} = (\varepsilon_\parallel - \varepsilon_\perp)\cos^2\theta + \varepsilon_\perp, \quad \varepsilon_{13} = (\varepsilon_\parallel - \varepsilon_\perp)\sin\theta\cos\theta, \quad \varepsilon_{11} = (\varepsilon_\parallel - \varepsilon_\perp)\sin^2\theta + \varepsilon_\perp.$$

Since in the thin sheet approximation the director angle θ is independent of the coordinate z perpendicular to the film to leading order (see (26)), so that ε_{33} is independent of z, the leading-order electric potential Ψ_0 satisfies

$$\Psi_0 = za(x) + b(x),$$

corresponding to an electric field (from (A 1))

$$\boldsymbol{E} = \Psi_{0z}\boldsymbol{e}_z + O(\delta) = a(x)\boldsymbol{e}_z + O(\delta).$$

Here $a(x)$ is arbitrary, although in practice the field will have to match to a solution of Maxwell's equations outside the nematic sheet via appropriate boundary conditions.

With the free energy density scaled with $K/(\delta^2 L^2)$, the dimensionless energy density W is then given by

$$2W = \theta_z^2 - \delta e(x)(\cos^2\theta + \lambda) + O(\delta^2),$$

where

$$e(x) = \frac{\delta L^2 E_0^2 \varepsilon_0 (\varepsilon_\parallel - \varepsilon_\perp)}{K} a(x)^2 = e_0 a(x)^2, \qquad \lambda = \frac{\varepsilon_\perp}{\varepsilon_\parallel - \varepsilon_\perp},$$

and $e(x)$ is assumed to be $O(1)$.

A.1 The required exterior field

The above relates to the electric field within the nematic sheet, but in practice we envisage an externally supplied electric field, which we write in terms of (dimensionless) electric potentials Ψ (inside the film; see above) and $\hat{\Psi}$ (outside the film); Ψ and $\hat{\Psi}$ scale differently, as discussed below. Outside the nematic sheet we assume the dielectric tensor ε_{ij} to be the identity tensor δ_{ij}. Then outside the sheet $\hat{\Psi}$ satisfies Laplace's equation, and the jump conditions across the air-nematic interface are (in the dimensional, unscaled

variables)

$$[\boldsymbol{v}^* \cdot \underline{\underline{\varepsilon}}^* \cdot \boldsymbol{E}^*] = 0, \quad [\boldsymbol{E}^* \cdot \boldsymbol{t}^*] = 0,$$

where $\boldsymbol{v}^*$ is the normal vector, and $\boldsymbol{t}^*$ is the tangent vector to the interface.

In the outer (air) region the geometry is no longer slender: both x^*- and z^*-coordinates scale with sheet length L^*, and we use dimensionless variables $(x, \hat{z})$ to denote this different scaling: $(x^*, z^*) = L^*(x, \hat{z})$, $\hat{z} = \delta z$. We then have Laplace's equation in $(x, \hat{z})$ for the electric potential $\hat{\Psi}$ (now made dimensionless by scaling with LE_0), and the above boundary conditions are applied, to leading order, on the line $\hat{z} = 0$. We only need consider $\hat{\Psi}$ in the region $\hat{z} > 0$ since we know the sheet geometry is symmetric about the x-axis, to leading order. With our knowledge of the scalings and solution in the slender sheet region, the problem for the leading-order potential $\hat{\Psi}_0$ is then

$$\nabla^2 \hat{\Psi}_0 = 0 \quad \hat{z} > 0,$$
$$\hat{\Psi}_{0x} = 0 \quad \text{on } \hat{z} = 0,$$
$$\hat{\Psi}_{0\hat{z}} = \varepsilon_{33}\Psi_{0z} = (\varepsilon_\parallel - \varepsilon_\perp)(\cos^2\theta + \lambda)a(x) \quad \text{on } \hat{z} = 0,$$

where, recall, θ is a prescribed function of $a(x)$ given by (26). We solve this problem by writing

$$(\cos^2\theta + \lambda)a(x) = A'(x), \tag{A 2}$$

and introducing a complex potential $f(Z)$, such that $\hat{\Psi}_0 = \Re(f(Z))$, with $Z = x + i\hat{z}$. Then on the boundary $\hat{z} = 0$ we have $f'(Z) = \hat{\Psi}_{0x} - i\hat{\Psi}_{0\hat{z}} = -i\varepsilon_a A'(x)$, that is,

$$f'(Z) = -i\varepsilon_a A'(Z) \quad \text{on } \Im(Z) = 0$$

(here we have introduced the dielectric anisotropy, $\varepsilon_a = \varepsilon_\parallel - \varepsilon_\perp > 0$). Provided $A'(Z)$ is analytical (it is at least in some neighbourhood of the real axis), this condition may be analytically continued away from this boundary, and we deduce that in fact

$$f(Z) = -i\varepsilon_a A(Z) + \kappa \quad \text{in } \Im(Z) > 0. \tag{A 3}$$

Hence, we have the (leading-order) electric potential and field everywhere; substituting for $\theta(x) = \theta_B g(a(x))$ from (26), we finally have

$$\boldsymbol{E}_{\text{ext}} = \nabla \hat{\Psi}_0 = \varepsilon_a \left(\Im((\cos^2(\theta_B g(a(Z))) + \lambda)a(Z)), \Re((\cos^2(\theta_B g(a(Z))) + \lambda)a(Z)) \right)$$
$$+ O(\delta), \tag{A 4}$$

with $g(a)$ given by (13).

To generate the required exterior field (A 4) we take the following steps: (i) Specify the function $a(x)$ characterizing the electric field within the sheet; (ii) calculate $A(x)$ (from (A 2)) and hence $A(Z)$; (iii) write down the complex potential $f(Z)$ from (A 3); (iv) find the (leading-order) electric potential $\hat{\Psi}_0 = \Re(f(Z))$; and (v) plot the level curves of $\hat{\Psi}_0$ (equipotentials). These equipotentials provide a family of possible electrode shapes that can be used to generate the desired $a(x)$, provided we choose two equipotentials so as to
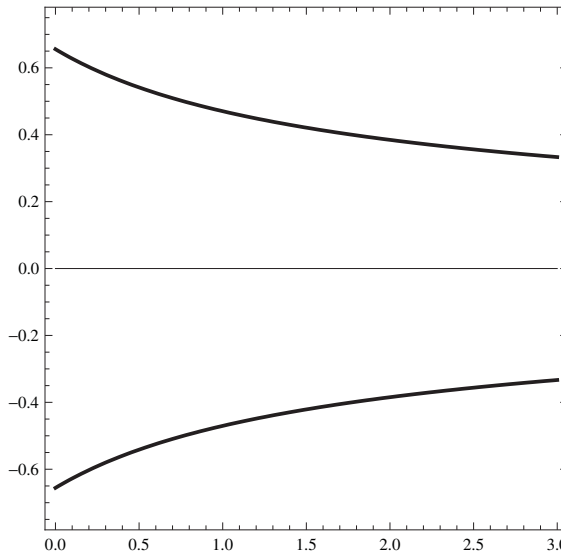
FIGURE A 1. Possible electrode shapes that could be used to generate the external field used for the examples given in Sections 3.1 and 3.2.1. The electrodes, which are equipotentials $\hat{\Psi}_0 = \pm 1$ and are represented by the thick black lines, surround the sheet, which lies along the horizontal (x) axis. With reference to Section 3.1, parameter values were chosen as: $E_F/\hat{N} = 1$; $\lambda = 1$ and $e_0 = 1$ in (18).

avoid any singularities of $\hat{\Psi}_0$ between them (this is possible because $A(Z)$ is guaranteed to be analytic at least in some neighbourhood of the real axis where the sheet lies).

Thus, our original assumption that we may choose the form of the electric field within the sheet is justified. To illustrate, we carry out the above procedure for the electric field chosen for the steady solutions of Section 3.1 (and used again for the first exact zero surface tension solution presented in Section 3.2.1). Two equipotentials of the resulting electric potential are shown in Figure A 1; these are possible electrode shapes that could be used to generate the electric field for those examples.

On the other hand, we can, of course, turn the problem around and ask the following: For a given external field satisfying $\hat{\Psi}_{0x}|_{\hat{z}=0} = 0$, what is the corresponding field within the nematic sheet? By way of illustration, suppose the external field is given by

$$\hat{\Psi}_0 = \frac{1}{2}\Re(-iZ^2) = x\hat{z}, \quad \boldsymbol{E}_{\text{ext}} = \hat{z}\boldsymbol{e}_x + x\boldsymbol{e}_{\hat{z}}, \tag{A 5}$$

which satisfies the boundary condition. (In line with the discussion above, hyperbolic electrode shapes could be used to generate such an external field.) The function $A(Z)$ is then given by $A'(Z) = Z/\varepsilon_a$, so the (leading-order) field within the sheet is $\boldsymbol{E} = a(x)\boldsymbol{e}_z$, where $a(x)$ satisfies

$$\frac{x}{\varepsilon_a} = a(x)\left[\cos^2\left(\frac{\theta_B E_a^2}{a(x)^2 + E_a^2}\right) + \lambda\right]. \tag{A 6}$$

Appendix B Contact angles

In this paper, when solving the non-zero surface tension problem, we assumed that the gradient of the sheet's free surface (related to the contact angle) was prescribed at the end-plates holding the bridge. In this appendix we derive a more general boundary condition on the contact angle, and specify conditions under which our assumption is valid.

In general it is known that a relationship exists between the dynamic contact angle $\phi(t)$ at a moving contact line and the speed of the moving contact line. While many such empirical relationships exist, a commonly used law (due to Cox and Voinov [3, 19]) takes the form

$$\phi^3 - \phi_e^3 = \kappa V_n \quad \text{at the contact line,} \tag{B 1}$$

where ϕ_e is the equilibrium contact angle for the given fluid–surface combination, κ is a constant having dimensions of time/length and V_n is the speed of the contact line in the direction of its motion (for our sheet, $V_n = h_t$). Since we are in the lubrication regime, we know that the slope of the sheet must always be small so that

$$\phi(t) = \frac{\pi}{2} - \delta\beta(t), \qquad \phi_e = \frac{\pi}{2} - \delta\beta_e.$$

Rewriting (B 1) in our dimensionless variables (14) and substituting for ϕ and ϕ_e, we obtain (at leading order and after dropping the tildes)

$$\beta_e - \beta = kh_t \quad \text{at the contact line;} \quad k = \frac{4}{3\pi^2}\kappa U.$$

Within our lubrication approximation we have $h_x = \phi_1$ to leading order, giving the boundary condition

$$h_x + kh_t = \beta_e \quad \text{at } x = s(t); \quad k = \frac{4}{3\pi^2}\kappa U.$$

An exactly similar analysis may be carried out at the left-hand boundary $x = 0$. In the simulations of this paper we have assumed $k \ll 1$ so that contact angles are approximately constant within our lubrication assumption.

References

[1] BUCKMASTER, J. D., NACHMAN, A. & TING, L. (1975) The buckling and stretching of viscida. *J. Fluid Mech.* **69**, 1–20.

[2] CHANDRASEKHAR, S. (1992) *Liquid Crystals*, 2nd ed., Cambridge University Press, Cambridge, UK.

[3] COX, R. G. (1986) Dynamics of the spreading of liquids on a solid surface, Part 1. Viscous flow. *J. Fluid Mech.* **168**, 169–194.

[4] DE GENNES, P. G. & PROST, J. (1993) *The Physics of Liquid Crystals*, 2nd ed., International Series of Monographs on Physics 83, Oxford Science Publications, Oxford, UK.

[5] HOWELL, P. D. (1994) *Extensional Thin Layer Flows*, DPhil thesis, University of Oxford, Oxford, UK.

[6] HOWELL, P. D. (1996) Models for thin viscous sheets. *Eur. J. Appl. Math.* **7**(4), 321–343.

[7] KING, J. R. & OLIVER, J. M. (2005) Thin film modeling of poroviscous free surface flows. *Eur. J. Appl. Math.* **16**, 519–553.

[8] LESLIE, F. M. (1979) Theory of flow phenomena in liquid crystals. *Adv. Liq. Cryst.* **4**, 1–81.

[9] LIN, T.-S., KONDIC, L., THIELE, U. & CUMMINGS, L. J. (2013) Modeling spreading dynamics of nematic liquid crystals in three spatial dimensions. *J. Fluid Mech.* **729**, 214–230.

[10] LIN, T.-S., KONDIC, L., THIELE, U. & CUMMINGS, L. J. (2013) Note on the hydrodynamic description of thin nematic films: Strong anchoring model. *Phys. of Fluids.* **25**(8), Art. No. 082102.

[11] OCKENDON, H. & OCKENDON, J. R. (1995) *Viscous Flow*, Cambridge University Press, Cambridge, UK.

[12] PALFFY-MUHORAY, P. (2007) The diverse world of liquid crystals. *Phys. Today.* **60**(9), 54–60.

[13] POULARD, C. & CAZABAT, A.-M. (2005) Spontaneous spreading of nematic liquid crystals. *Langmuir* **21**, 6270–6276.

[14] REY, A. D. & CHEONG, A.-G. (2004) Texture dependence of capillary instabilities in nematic liquid crystalline fibres. *Liq. Cryst.* **31**, 1271–1284.

[15] SAVAGE, J. R., CAGGIONI, M., SPICER, P. T. & COHEN, I. (2010) Partial universality: Pinch-off dynamics in fluids with smectic liquid crystalline order. *Soft Matter*, **6**, 892–895.

[16] SMOLKA, L. B., BELMONTE, A., HENDERSON, D. M. & WITELSKI, T. P. (2004) Exact solution for the extensional flow of a viscoelastic filament. *Eur. J. Appl. Math.* **15**, 679–712.

[17] STEWART, I. W. (2004) *The Static and Dynamic Continuum Theory of Liquid Crystals: A Mathematical Introduction*, Taylor & Francis, New York, NY.

[18] VAN DE FLIERT, B., HOWELL, P. D. & OCKENDON, J. R. (1995) Pressure-driven flow of a thin viscous sheet. *J. Fluid Mech.* **292**, 359–376.

[19] VOINOV, O. V. (1977) Hydrodynamics of wetting. *Fluid Dyn.* **11**(5), 714–721.